D. L. Wertz
W. T. Mealor
M. L. Steele
J. W. Pinson
University of Southern Mississippi
Hattiesburg, MS 39401

Correlation between Multispectral Photography and Near-Surface Turbidities*

An empirical relationship between spectral response in four-band multispectral photography and near-surface turbidities in the Ross Barnett Reservoir was found.

Abstract: *Four-band multispectral photography, obtained from an aerial platform at an altitude of about 10,000 feet, has been utilized to measure near-surface turbidity at numerous sampling sites in the Ross Barnett Reservoir, Mississippi. Correlation of the composited photographs with turbidity measurements has been accomplished via an empirical mathematical model which depends upon visual color recognition when the composited photographs are examined on either an I²S model 600 or a Spectral Data model 65 color-additive viewer. The mathematical model was developed utilizing least-squares, iterative, and standard statistical methods and includes a time-dependent term related to sun angle. This model is consistent with information obtained from two overflights of the target area–July 30, 1973 and October 30, 1973–and now is being evaluated with regard to information obtained from a third overflight, on November 8, 1974*

Introduction

During the past decade, the description and measurement of hydrographic and aquatic systems through remote sensing techniques has become the focus of a significant amount of scientific research. Although several researchers have correlated and modeled the spectral signatures of various water parameters, few have attempted quantitatively to correlate turbidity with multispectral photography. This paper presents a technique and model for correlating turbidity with composite multispectral photographs.

The Test Site

The test site for this project is the Ross Barnett Reservoir, a man-made lake of less than 40 feet maximum depth, on the outskirts of Jackson, Mississippi. The 30,000 acre reservoir, completed in the early 1960's by damming the Pearl River, is a focus not only for recreational use, but also for residential growth. More than 200 new houses have been built in restricted subdivisions

* A portion of this work was discussed at the Ninth International Symposium on Remote Sensing of the Environment, Ann Arbor, Michigan, April 1974.

bordering the reservoir since 1968. In addition to residential and recreational uses, cotton and soybean production, traditionally characteristic of this area, occurs within 100 yards of some areas of the shoreline.

Although this paper concerns only one parameter of water quality, the Ross Barnett Reservoir remote sensing project, a multidisciplinary research effort, is much broader in context and spatial scope, dealing with land use, sedimentation, water quality and their interrelationships over approximately 20 square miles. Data for this paper was acquired from two distinct areas of the reservoir study area, Alford Cove and Fannin Landing, each smaller than 2 square miles in size (Figure 1).

Alford Cove, the smaller of the two sites, is located adjacent to a recently developed subdivision. Homes within the development have been constructed since 1968, and each occupies a relatively large and heavily wooded lot. The majority of the homes having frontage on the water also have boat docks. Alford Cove has been repeatedly dredged in order to permit usage of pleasure craft. The Fannin Landing area is characterized by cotton production, planted pine, mixed hardwood-pine forests, and recreational uses, all within 100 yards of the shoreline. The shoreline in the vicinity of the boat ramp at Fannin Landing is similar to the shoreline in Alford Cove: both resemble submergent forms, with 18 inches to 2 feet of vertical relief between the water surface and adjacent land. However, in the cotton fields area along the north shore of Fannin Landing slopes are gentle and there is no sharp relief discontinuity between water surface and land. Also, the vegetation milieu along the cotton fields shore consists of a variety of aquatic and wetlands species not found in Alford Cove or elsewhere at Fannin Landing. Water craft activities at Fannin Landing are considerably less than in Alford Cove.

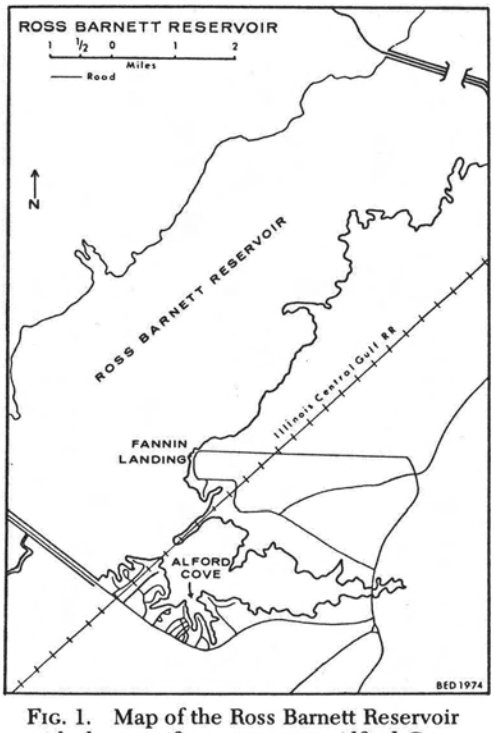

FIG. 1. Map of the Ross Barnett Reservoir with the specific target areas, Alford Cove and Fannin Landing, indicated.

Water sampling sites were selected in Alford Cove and in the Fannin Landing vicinity to correspond with a variety of onshore land uses with the objective of relating land use with sedimentation and water quality. A series of water sampling points, shown in Figures 2 and 3, were established in grid patterns initiated within a few feet of the shore to more than one-quarter mile from the shore. This pattern of water sampling points provided a means of monitoring and distinguishing near shore phenomena from phenomena which characterize more open water.

Water Sampling

Near-surface water temperature, secchi disc visibility, and relative humidity were measured at each site. At each site samples were taken for turbidity, apparent water color, conductivity, and suspended sediment load measurements. The latter two were conducted in our laboratories several days after each overflight, but turbidity and apparent water color measurements were conducted at the reservoir within two hours of the time the samples were taken. During this two-hour interval the samples were stored in covered ice chests at 0°C to 5°C in order to minimize changes in turbidity in the samples. Turbidities, apparent water colors, and conductivities were measured with a Hach DR/2 Field Spectrophotometer.

Suspended solids were measured by filtering and subsequently evaporating to a constant weight a 4 liter sample which had been taken near the water surface.

Camera and Imagery Format

Imagery utilized in this study was generated via a 100mm focal length I²S multiband camera loaded with Eastman black-and-white infrared film type 2424. The respective bands (blue, green, red, and near in-

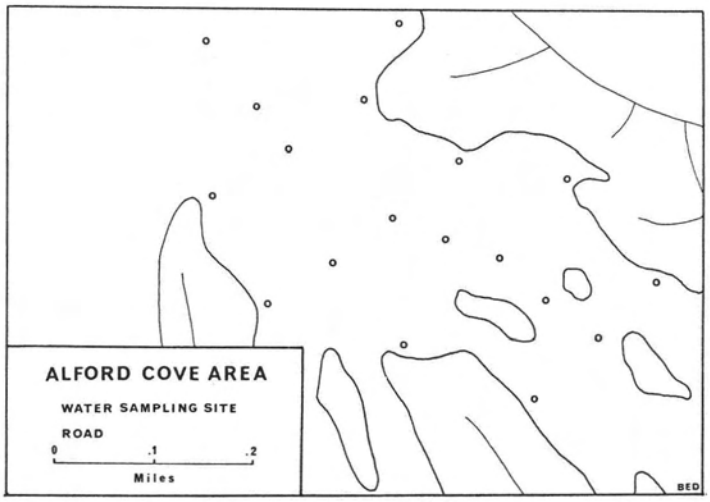

FIG. 2. Water Sampling Sites in the Alford Cove Region. Sampling Sites are depicted by ○.

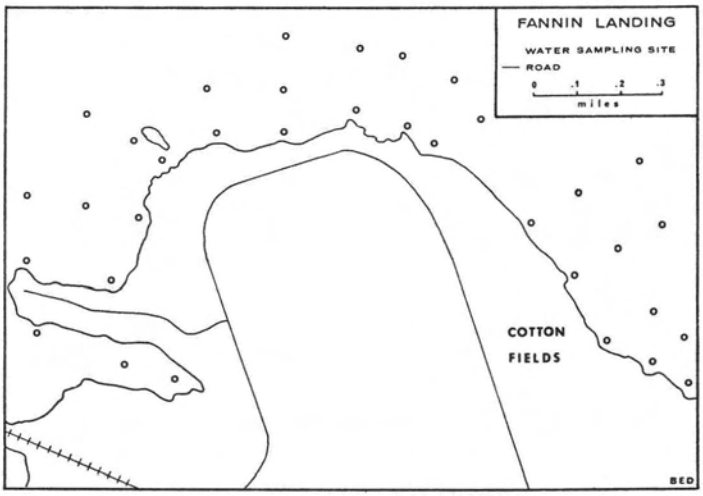

FIG. 3. Water Sampling Sites in the Fannin Landing Region. Sampling Sites are depicted by ○.

frared) were filtered through 47B, 57A, 25, and 88A filters. The sensor package was flown at 10,000 feet, yielding a negative scale of approximately 1:33,000. Imagery scale when viewed on the I²S Mini-Addcol Model 600 color additive viewer was approximately 1:13,200. When viewed on a Spectral Data Model 65 color additive viewer, the negative scale was enlarged to approximately 1:10,200. Both viewers were utilized in this study.

MISSIONS

Seven photographic missions were flown prior to January 1, 1974. Of these, several produced multispectral photographs which were not suitable for analysis. One mission produced photographs which were of high quality but did not include enough of the sample sites to be statistically useful in this study. Consequently this study is based upon photographs obtained from two missions—July 30, 1973 and October 30, 1973. High quality photographs obtained from a mission flown on November 8, 1974 are currently being analyzed.

Atmospheric conditions for both flights were satisfactory. Rainfall in the vicinity of

the test site was less than 0.5 cm during the week prior to the July 30 mission. Winds were from southwest to west at 5 knots, surface temperatures were 25-30 °C and relative humidity was 70-75 per cent. Near-surface water temperatures ranged from 30-32 °C. Test site weather conditions for the October flight also were good. At the time of the overflight surface winds were from the west at 6 knots, the temperature was 20-25 °C, and relative humidity was in the mid 40's. Near-surface water temperature ranged from 19 to 21 °C. Two days previous to the October overflight, 1.0 cm of rain fell in the vicinity.

Imagery Analysis

Sequential seasonal imagery posed two problems, both of which had to be rationalized in order to correlate turbidity with signature of composite multispectral imagery. The first problem concerned the compatibility and comparability of the tonal signature of each imagery set. Second, consistency in signature registration of composite multispectral photographs on the color additive viewer had to be achieved between the two sets of imagery. Inspection of the film indicated that both sets of imagery were of good tonal contrast and that the tonal signatures obtained were compatible. Even though there were some color shifts due to both seasonal variations and film quality, the correlations necessary for construction of the predictive model (shown below) were not hindered. The authors feel that perception of any color shifts on our imagery was due to seasonal conditions rather than film or viewer variations.

A third problem related to film quality is the necessity of having imagery that, when viewed on a color additive viewer, produces high contrast. Even in the analysis of one roll of imagery, it is necessary to have good contrast in order to produce optimum correlation of composite photograph signatures with measured turbidities at numerous sample sites. Needless to say, sun glint is unwanted. For that reason both missions were flown at approximately 9:45 A.M., local time, so that sun glint was minimized.

The procedure which allows mathematic correlation of composited multispectral photographs with measured near-surface water turbidities was based upon two criteria: (1.) that optimum color contrast is obtained with the color additive viewer; and (2.) that water depth effects can be ignored.

These criteria are satisfied when the spectral responses of the water are displayed on a color additive viewer between 600 nm and 750 nm, though in all likelihood other spectral regions would be as satisfactory.

The spectral regions from 600 nm to 750 nm was separated into nine color zones, each readily discernible to the human eye and distinguishable from the other color zones. The median wavelength, $\bar{\lambda}$, for each color zone was used to represent that color zone in subsequent modeling. The color zones are described in Table 1.

Correlations and Modeling

The following technique was developed to investigate the multispectral photographs.

1. For the Alford Cove (AC) and the Fannin Landing (FL) sites, the graphs of turbidity versus $\bar{\lambda}_i$ (Figures 4 and 5) were analyzed by least

Table 1. A Description of the Color Zones.

Color Zone	λ_{max}	λ_{min}	$\bar{\lambda}$
1	750	738	744
2	738	712	725
3	712	680	696
4	680	666	673
5	666	654	660
6	654	642	648
7	642	630	636
8	630	616	623
9	616	600	608

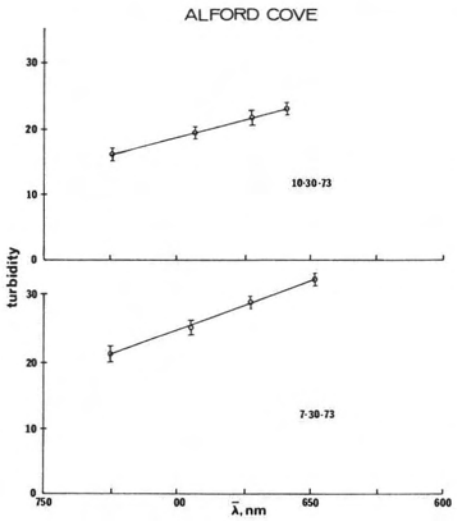

Fig. 4. Graphical correlation of measured near-surface turbidity values for samples from Alford Cove with $\bar{\lambda}_i$ for the two overflights. Error bars represent the 95 per cent confidence level.

squares methods. The slope of turbidity versus $\bar{\lambda}_i$ for the 7-30-73 imagery was 0.174 STU/nm whereas, for the 10-30-73 imagery, the slope was 0.129 STU/nm. For the spectral region from 750 nm to 680 nm for the Fannin Landing sites, the slope of turbidity versus $\bar{\lambda}_i$ was 0.123 STU/nm for the 7-30-73 imagery and 0.091 STU/nm for the 10-30-73 imagery.

2. It was assumed that each slope represents the product of an empirical constant ß and the sun angle term ϕ_a. Solutions to the four equations

$$\beta_{AC} \times \cos \phi_{a_1} = 0.175 \text{ STU/nm},$$
$$\beta_{AC} \times \cos \phi_{a_2} = 0.129 \text{ STU/nm},$$
$$\beta_{FL} \times \cos \phi_{a_1} = 0.123 \text{ STU/nm, and}$$
$$\beta_{FL} \times \cos \phi_{a_2} = 0.091 \text{ STU/nm},$$

were determined by iterative computer methods according to two criteria: minimize $\sum \rho_i^2$ and minimize $\sum Q_i^2$. Equal weighting was given to both restrictive conditions. Since both summations were minimized in the vicinity of the values for ß and ϕ_a shown below, it was assumed that these values were satisfactory. Furthermore, since $(\beta_{FL} \cos \phi_{a2}/\beta_{AC} \cos \phi_{a2}) = (\beta_{FL} \cos \phi_{a2}/\beta_{AC} \cos \phi_{a2})$, the assumption noted above was justified. In the equations the subscripts 1 and 2 refer to the information obtained from the 7-30-73 and the 10-30-73 overflights, respectively.

3. Having determined suitable values for ß and ϕ_a for the Fannin Landing sites, the value of χ was determined from the second slope (in the vicinity from 660 nm to 600 nm) again by least squares methods. For the 7-30-73 imagery $\chi_1 = (0.181 \text{ STU/nm})/\cos \phi_{a1}$ and for the 10-30-73 imagery $\chi_2 = (0.158 \text{ STU/nm})/\cos \phi_{a2}$. The values of χ determined from these two equations differed by < 1 per cent so the mean value of χ was utilized in subsequent calculations.

4. The minimization step outlined above was repeated to obtain optimum values of ß, χ, and ϕ_a for each sampling region and for each overflight. These values are shown in Table 2.

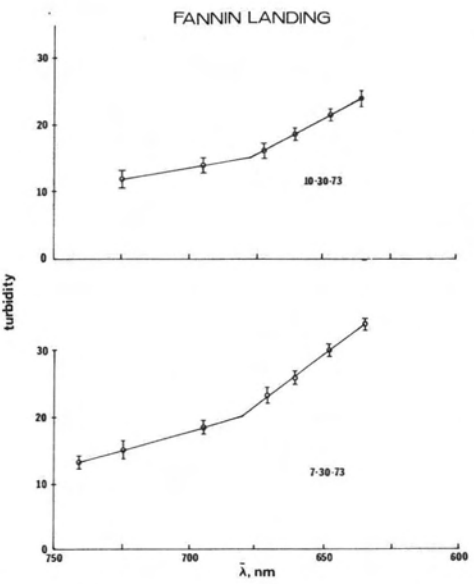

FIG. 5. Graphical correlation of measured near-surface turbidity values for samples from the Fannin Landing region with $\bar{\lambda}_i$ for the two overflights. Error bars represent the 95 per cent confidence level.

TABLE 2. BEST FIT VALUES.

Location		β	χ	ϕ_a
Alford Cove Sites	7-30-73	0.210	0.000	33.6
	10-30-73	0.210	0.000	54.1
Fannin Landing Sites	7-30-73	0.148	0.217	33.6
	10-30-73	0.148	0.217	54.1

On the basis of these empirically derived relationships, we have developed a model which relates visually interpreted multispectral photography to measured near-surface turbidity.

The model that we have developed is

$$\xi_i = \{\beta(\lambda^* - \bar{\lambda}_i) + \delta\chi(\kappa - \bar{\lambda}_i)\} \cos \phi_a$$

or

$$\lambda_i = [\beta + \delta\chi\kappa - t_i/\cos \phi_{an}] \cdot$$

In these equations ξ_i is the turbidity calculated via the model at the sample site i, $\bar{\lambda}_i$ is the wavelength representing the color zone of the composite photography at site i, and λ_i is the spectral response anticipated for the ith sampling site. Other terms are defined below. Because of calm, clear weather conditions between 9:00 A.M. and 10:00 A.M. (local time) on the days of the overflights, wave heights in the reservoir were less than 2 cm. Consequently the model is not complicated by wave effects; i.e., a glassy surface model realistically represents the water surface on the days of these overflights.

The model has been utilized to examine turbidity versus spectral response correlations for a third overflight date. Whereas correlation is satisfactory, too few turbidity values were measured to allow inclusion of these data and calculations.

Shown in Table 3 are comparisons of the measured turbidities and the turbidities calculated via our model for the two overflights.

CONCLUSIONS

An empirical, three parameter equation which includes a sun angle (time) term has been shown to correlate composited four-

TABLE 3. COMPARISON OF MEASURED AND CALCULATED TURBIDITIES.

Site Number	July 30, 1973 Color Zone	t_i	ξ_i	ρ_i	October 30, 1973 Color Zone	t_i	ξ_i	ρ_i
Fannin Landing Sites								
31	3	18	19	1	2	12	11	1
32	3	18	19	1	3	14	13	1
35	1	13	13	0	4	16	16	0
34	3	20	19	1	2	11	11	0
35	3	20	19	1	2	11	11	0
40	4	23	24	1	4	16	16	0
41	3	19	19	0	4	18	16	2
42	3	20	19	1	3	14	13	1
42A	3	19	19	0	4	15	16	1
47	7	34	35	1	6	21	22	1
47A	3	19	19	0	6	21	22	1
47B	2	16	15	1	5	19	18	1
48	3	17	19	2	5	18	18	1
48A	2	15	15	0	4	16	16	0
49	6	30	30	0	7	24	24	0
49A	3	18	19	1	6	22	22	0
49B	3	17	19	2	5	19	18	1
Alford Cove Sites								
1	3	26	25	1	3	20	19	1
2	4	28	29	1	2	16	15	1
3	4	28	29	1	3	19	19	0
4	4	30	29	1	3	18	19	1
5	3	26	25	1	2	18	15	3
6	4	30	29	1	3	19	19	0
7	4	30	29	1	3	20	19	1
8	3	28	25	3	3	19	19	0
9	4	30	29	1	3	20	19	1
10	4	29	29	0	3	19	19	0
11	5	32	24	2	4	22	22	0
12	3	26	25	1	4	21	22	1
13	4	28	29	1	3	20	19	1
14	3	26	25	1	4	21	22	1
15	3	24	25	1	4	21	22	1
16	2	22	20	2	4	21	22	1
17	3	23	25	2	4	22	22	0
18	2	20	20	0	3	20	19	1
19	3	25	25	0	4	22	22	0

band multispectral photographs with measured near-surface turbidity values at numerous sampling sites in the Ross Barnett Reservoir. The model correlates the measured turbidities (t_i) with the spectral responses ($\bar{\lambda}_i$) at the various sample sites; and a first order relationship between the color signature of the sampling site ($\bar{\lambda}_i$) and the turbidity exists as shown above. It has been shown, however, that the spectral response-turbidity relationship for the the Alford Cove sites differs somewhat from that determined for the Fannin Landing sites.

An important contribution of this study is that the turbidity-spectral response correlations can be made. Though this model has not been tested on other fresh water bodies, it is the opinion of the authors that under similar physiographic and climatic conditions, our model relating turbidity to color response of the composited four-band multispectral photographs will be applicable and highly useful.

ACKNOWLEDGMENTS

This research was supported by the National Aeronautics and Space Administration's University Relations Office via contract number NGL25-005-007. The authors also gratefully acknowledge the support of the NASA Earth Resource Laboratory, National Space Technology Laboratories which obtained the photography cited in the text.

LIST OF DEFINITIONS

COLOR ZONE. A region of the visible spectrum which is discernible and distinguishable. A color zone has two wavelength boundaries, λ_{max} and λ_{min}, and a median wavelength, $\bar{\lambda}$.

$\bar{\lambda}$—The wavelength used to represent a particular color zone.

λ^*—The high wavelength intercept on the graphs of turbidity versus spectral response, about 840 nm.

t_i—The turbidity measured at the ith sampling site in standard turbidity units (STU).

$\bar{\lambda}_i$—The color zone representation of the ith sampling site as determined from the imagery.

ξ_i—The turbidity calculated for each sampling site from our model. The only inputs into the model are $\bar{\lambda}_i$ for each sampling site and the empirical constants. (See below).

λ_i—The anticipated spectral response of the viewed multispectral photograph as calculated by our model.

κ—An empirical constant, about 680 nm. At about 680 nm, the slope of turbidity versus $\bar{\lambda}_i$ changes in the multispectral photographs of the Fannin Landing sites.

ϕ_a—Sun-site-camera angle; equal to $\pi/2$ minus the sun angle.

δ—The Dirac delta function; equal to 1.0 when $\bar{\lambda}_i < \kappa$ and equal to 0.0 when $\bar{\lambda}_i > \kappa$.

$\rho_i - \rho_i = |t_i - \xi_i|$

$Q_i - Q_i = |\lambda_i - \bar{\lambda}_i|$

REFERENCES

Blanchard, Bruce J., and Ross W. Leamer, 1973. "Spectral Reflectance of Water Containing Suspended Sediment," In *Remote Sensing and Water Resources Management*. Keith P. B. Thomson, Robert K. Lane, and Sandor C. Csallany, editors, 339-347.

Brown, W. l., *et al.*, 1972. "Calculating Water Quality Parameters Using Remotely Sensed Scanner Data." *Proceedings* of the Eighth International Symposium on Remote Sensing of Environment, 563-567.

Carlson, P. R. and D. S. McCulloch, 1974. "Aerial Observations of Suspended Sediment Plumes in San Francisco Bay and the Adjacent Pacific Ocean." *J. Research U.S. Geol. Survey*, 2(5): 519.

Klemas, V., *et al.*, 1974. "Correlation of Coastal Turbidity and Circulation with ERTS-1 and Skylab Imagery," *Proceedings* Ninth International Symposium on Remote Sensing of the Environment, Ann Arbor, Michigan, 1289-1318.

Ritchie, Jerry C., *et al.*, 1974. "The Relationship of Reflected Solar Radiation and the Concentration of Sediment in the Surface Water of Reservoirs," Presented at the Third Annual Remote Sensing of the Earth Resources Conference, Tullahoma, Tennessee.

———., 1975. "Sun Angle, Reflected Solar Radiation, and Suspended Sediments in North Mississippi Reservoirs," Presented at the Fourth Annual Remote Sensing of the Earth Resources Conference, Tullahoma, Tennessee.

Scherz, J. P., 1971. "Remote Sensing Considerations for Water Quality Monitoring." *Proceedings* of the Seventh International Symposium on Remote Sensing of Environment, 1071-1088.

Schiebe, Frank R., and Jerry C. Ritchie, 1975. "Color Measurements and Suspended Sediments in North Mississippi Reservoirs," Presented at the Fourth Annual Remote Sensing of the Earth Resources Conference, Tullahoma, Tennessee.

Taras, M. J., *et al.*, 1971. *Standard Methods for the Examination of Water and Waste Water.* Am. Pub. Health Asso., Washington, D.C., 349-359.

Wezernak, C. T., and F. C. Polcyn, 1972. "Eutrophication Assessment Using Remote Sensing Techniques." *Proceedings* of the Eighth International Symposium on Remote Sensing of Environment, 541-551.

Yarger, H. L., *et al.*, 1974 "Quantitative Water Quality with ERTS-1," *Proceedings* Third Earth Resources Technology Satellite Symposium, 1637.

Young, H. D., 1962. *Statistical Treatment of Experimental Data.* McGraw-Hill Book Company, New York.

Engineering Reports

Business—Equipment—Literature

Gordon R. Heath

Instronics Announces New Keyboard Cursor for Digitizing Hydrographic Maps and Charts

A "Keyboard Cursor" which facilitates the entering of numerical data while digitizing maps and charts has been introduced by Instronics for use with the Gradicon free cursor digitizer. A keyboard has been built right into the new cursor, permitting the operator to perform all digitizing and data entry functions directly from the cursor.

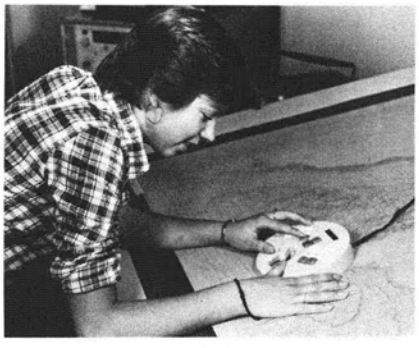

The new cursor is used to locate and follow the scribe marks on the mylar film normally used for hydrographic maps and charts. The Gradicon digitizer senses the cursor position and converts the coordinate data into digital form for computer processing. The cursor keyboard permits numerical data, such as depth soundings, to be entered concurrent with coordinate data. While specifically designed to enter depth soundings when digitizing hydrographic maps and charts, the new cursor can also be used in any digitizing application where entry of numerical data is required. Complete details on the new "Keyboard Cursor" are available from Instronics Inc., One Regency Drive, Bloomfield, CT 06002. Telephone (203) 242-2219.

Kern Instruments, Inc., Announces the Availability of Its New DC2 Interacting Digitizing-Graphic System

Kern Instrument's DC2 interacting digitizing graphic system, in conjunction with the PG2-AT stereoplotter, offers the user expanded semi-automatic plotting capabilities as well as significant compilation capability. The DC2 utilizes a